Available online at www.sciencedirect.com

Manufacturing Letters

Manufacturing Letters 44 (2025) 453–465

53rd SME North American Manufacturing Research Conference (NAMRC 53, 2025)

Optimizing Formability of Incremental Sheet Forming using the Straight Groove Test assessed with a Variable Wall Angle Conical Frustum

Ravi Prakash Singh[a,*], Santosh Kumar[c], Edward James Brambley[a,b], Sudarshan Choudhary[d], Pankaj Kumar Singh[c], Sisir Dhara[b]

[a]*Mathematics Institute, University of Warwick, Coventry CV4 7AL, UK*
[b]*WMG, University of Warwick, Coventry CV4 7AL, UK*
[c]*Department of Mechanical Engineering, IIT (BHU), Varanasi, U.P.-221005, India*
[d]*Department of Mechanical Engineering, SVNIT, Surat, Gujarat, India*

Abstract

The current study is focused on Robot Assisted Incremental Sheet Forming (RAISF) of AA 6061 alloys. A simple and streamlined approach is presented to optimize the forming parameters to maximize formability during RAISF; the forming parameters are the tool speed, the step depth, and the tool diameter. The optimized parameters are found using a Design of Experiments (DOE) methodology applied to a straight groove test. Straight groove tests were conducted on 39 samples chosen according to a Central Composite Response Surface Design (CCRSD) methodology. Formability is assessed by considering the groove depth, spring back, and forming time; the combination of tool speed (84.65, mm/s), tool diameter (12.5 mm) and step depth (0.4 mm) were found optimal. A Variable Wall Angle Conical Frustum (VWACF) was then fabricated to assess the effect of the optimized parameters on the limiting conical wall angle. Finally, a conical frustum of constant wall angle 60° was fabricated, and its forming limit compared with the conventional forming limit of AA 6061 obtained by a Nakajima test.

Keywords: Incremental forming; Straight groove test; Response surface; Optimization; Nakajima Test; Forming Limit Diagram

1. Introduction and Literature Review

Incremental sheet forming (ISF) is a flexible sheet forming process that offers several advantages over conventional forming techniques, such as reduced tooling costs, enhanced geometric flexibility, and the ability to produce complex shapes with minimal setup time [1, 2]. In this procedure, plastic deformation of sheet is performed gradually without the need for specialized dies; ISF is therefore termed a die-less forming technique [3, 4, 5]. Plastic deformation occurs through a series of incremental steps, with a small area of sheet under direct tool contact undergoing deformation at a time. Consequently, the deformation in ISF is characteristically gradual, localized, and of an incremental nature, contributing to improved formability limits compared with conventional sheet metal forming operations such as stamping and stretching [6, 7]. In a typical ISF process, the forming tool is mounted on a CNC machine [8, 9] or a robotic arm [10, 11] which gradually deforms the clamped sheet in a stepwise manner. The formability and quality of the final product are influenced by various input variables, including the tool diameter, step size, tool speed, and forming temperature [12, 13]. Numerous studies have been carried out to investigate the influence of input parame-

* Ravi Prakash Singh. Tel.: +44-758-659-2739.
E-mail address: ravi.p.singh@warwick.ac.uk (Sisir Dhara).

ters in ISF and their optimization to achieve a combination of superior formability and enhanced product quality [14, 15]. Shim and Park [16] recommended a standard test for plotting Forming Limit Curves (FLC) in major–minor strain space to predict formability during ISF, and this was utilized by Ham and Jeswiet [17] to study the formability of AA 3003. Similarly, Kim and Park [18] utilized a straight groove test to study the impact of various parameters on formability in ISF by conducting a series of experiments. Their findings revealed that increasing the tool size has a negative impact on the maximum forming angle of a fixed wall angle conical frustum. In contrast, Kumar et al. [19] investigated the influence of different parameters on the formability of AA 2024-O and reported that formability improves with larger tool diameters and the side radius of flat-end tools.

Although several studies have explored the impact of step size on formability, the effect of step size on sheet formability in ISF remains inconclusive. Some researchers have reported that increasing the step size has a negative effect on formability [20, 21, 22], whereas others have reported a positive effect of increasing step size on formability [23]. Furthermore, Ham and Jeswiet [17] suggested that step size has little effect on the maximum forming angle in ISF. Similarly, peripheral tool speed is another key factor affecting formability in ISF. Higher tool speeds lead to increased frictional heating [24], which softens the sheet material locally in contact with the tool and consequently enhances formability [25, 26]. Ham and Jeswiet [17], in their work on Aluminium alloy 3303 sheet, found increased formability with increasing speed. Similar results were obtained by Buffa et al. [27], who performed ISF at higher speeds on AA1050-O, AA1050-H24, and AA6082-T6. Xu et al. [28] explored the localized heating mechanism due to the relative motion at the tool-workpiece interface, resulting from tool rotation. Their experiments on AA5052-H32 sheets, with tool rotational speeds ranging from 0 to 7000 RPM, revealed that at lower speeds (0-1000 RPM), friction is the dominant factor, while at higher speeds, dynamic recrystallization effects take over. This explains why improved formability is typically observed at higher spindle speeds in ISF. In addition to this high speed ISF can also impact the surface quality of the formed product and several studies have been conducted to find out this effect [29]. The discussion above illustrates that several factors collectively influence formability in ISF. To better understand these effects and optimize the process for different material design of experiments (DOE) can be a powerful tool. This can enable a systematic evaluation of various parameters, helping to identify the optimal combination that can yield the best formability results [24].

The literature review indicates that, despite extensive research on the effects of various forming parameters on ISF process formability, the results remain inconclusive and subject to debate. Additionally, these findings are often material- and process-dependent. There is no documented test for selection of parameters and formability evaluation in ISF. This article presents a simplified but innovative approach for optimization of parameters using simple Straight groove test and formability evaluation using Variable Wall Angle Conical Frustum (VWACF). A standard straight groove test was employed to evaluate the impact of tool diameter, Step size, and peripheral speed on the formability and spring back in grooves formed during ISF on AA 6061. 39 different set of experiments were conducted, and the results were analysed using central composite response surface methodology. The effects of various parameters were studied and combination of these input parameters were chosen for optimum results. These set of parameters were chosen to fabricate VWACF for finding the limiting wall angle for fabrication of conical frustum which is a standard shape for testing in ISF. The strain in the plane of the fabricated cone was analysed on Major strain - Minor strain space was compared with the forming liming diagram of AA6061 for different strain paths.

2. Straight Grove Tests

The experimental setup for ISF as shown in figure 1 was developed from scratch and patented [30] at IIT BHU using a 6 axis industrial robot. This version of ISF process has been named Robot Assisted Incremental Sheet Forming (RAISF)[31]. Details of the experimental setup can be found in the previous studies by the authors [6, 32]. This setup was used to perform various forming operations on AA 6061, Chemical composition of which determined by optical emission spectrometer has given in Table 1. For finding out the mechanical properties of the undeformed, annealed sheet,uniaxial tensile test was performed on a 100 kN INSTRON (MODEL 8801) using samples as per the ASTM/E8 standard [33]. For studying the formability of the AA6061 sheet after heat treatment, Erichsen ductility test was conducted. The specimens were prepared as per the ASTM/E643/15 standard [34]. The diameter of indenter was 20mm with main scale division 1 mm, and the circular scale division of 50/5MSD. Three domes were formed by the indenter until the onset of fracture of the dome, and the depth of the indentation was measured as (H_D). The tensile properties and the details of the depth of indentation (H_D) of all the domes on the samples of AA6061 preform is presented in Table 2. As different forming parameters affect the forming outcomes in ISF, the optimization of these parameters is of significant importance. Several tests have been reported by different researchers to calculate the formability in ISF like VWACF [26] VWAPF [35] and forming limit for diffrent loading paths [36]. In the current study, a straight groove test [12] has been carried out, to op-

1'.png

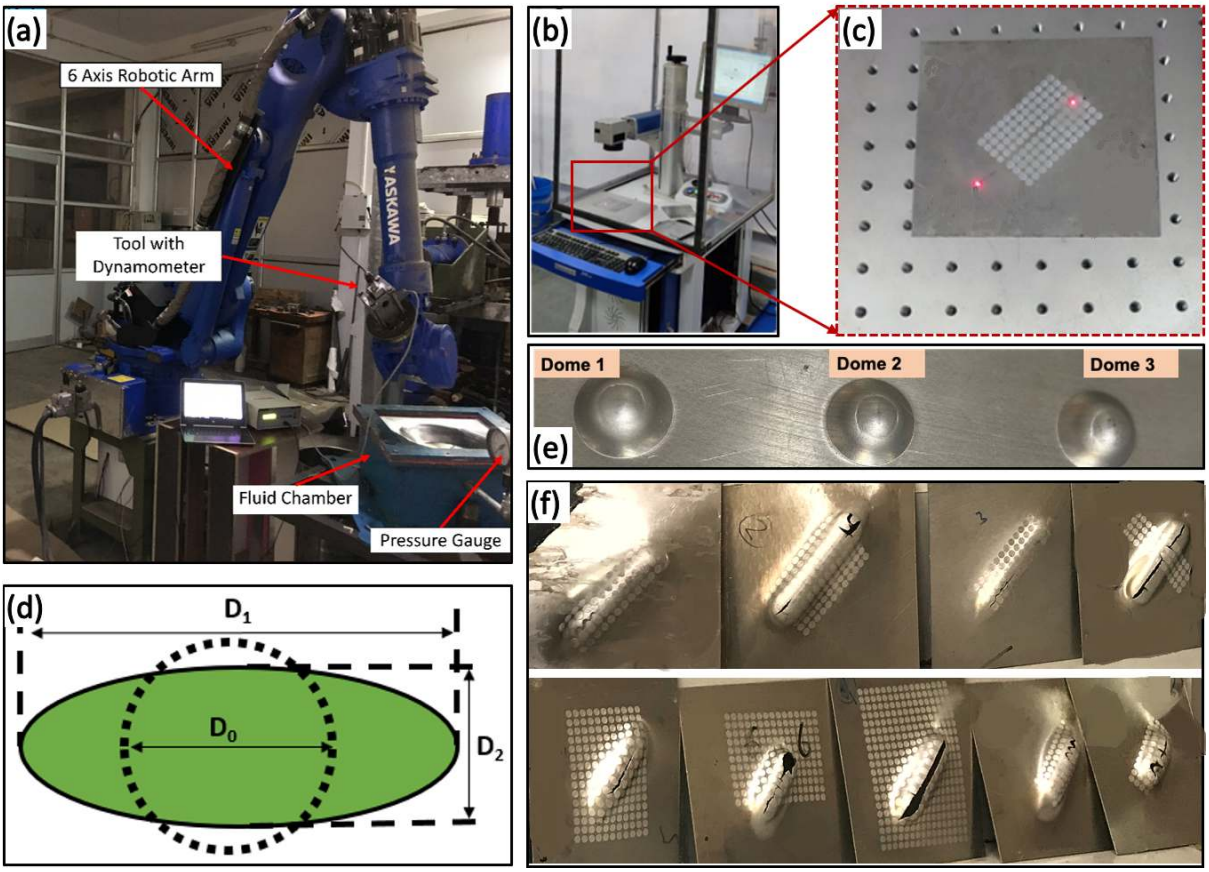

Figure 1: (a) RAISF setup at IIT, Varanasi (b) Laser Engraver for imprinting metallic sheets (c) Sheet Engraved with circular grid pattern (d) Measurement of Ellipse transformed from circle. (e) domes fabricated for Erichsen ductility test (f) formed grooves on Al6061 sheet

Elements	Al	Ti	Si	Mg	Fe	Mn	Zn	Cr	Cu
Composition (wt.%)	97.35	0.05	0.510	0.95	0.41	0.02	0.06	0.15	0.490

Table 1: Composition of the aluminium alloy AA6061

Tensile Properties		**Erichsen ductile properties**			
Properties	Values		Dome 1	Dome 2	Dome 3
Yield Strength(MPa)	112 ± 0.5	IE	9.34	9.12	8.92
UTS (MPa)	127 ± 0.5	Dome height (H_D)	9.02	8.82	8.61
Elongation(%)	14.50 + 0.1	Average H_D		9.13	

Table 2: Tensile and Erichsen ductility property of AA6061

timize tool diameter(d), step size (ΔZ) and tool speed (V) due to its simplicity, cost-effectiveness, and efficiency in delivering rapid results. In this procedure, a sheet blank is clamped on the basic fixture, and a straight groove is formed through the back-and-forth passes of the tool followed by a downward increment at the beginning of each pass of the forming tool equal to the step size (ΔZ). As the tool moves back and forth as well as in downward direction a straight groove is formed, the depth of which gives an idea of the formability achieved in the process. For optimization of input parameters, the Central Composite Response Surface Design (CCRSD) with $\alpha = \sqrt{2}$, , was used on Minitab software. For running the experiments, tool speed and step size were chosen as the continuous variables and Tool diameter was taken as a categorical variable. The details of the input parameters are given in Table 3. As can be seen from Table 3, three categorical levels of tool diameter viz. 10 mm, 12.5 mm and 15 mm were chosen along with continous variables of tool speed

Input Parameters	Type of parameters	Units	Levels
Tool speed	*Continuous*	*mm/s*	50 100
Step size	*Continuous*	*mm*	0.2 0.6
Tool diameter	*Categorical*	*mm*	10 12.5 15

Table 3: Input parameters for straight groove test

renging between 50 mm/s to 100 mm/s and step size ranging from 0.2 mm to 0.6 mm [18, 37]. The design of experiments based on CCRSD is detailed in Table 4. In this experimental series, four experiments were conducted at each tool diameter level, corresponding to the corner points of the central composite design, as indicated by experiment numbers (1-4), (14-17), and (27-30). Similarly, experiment numbers (5-8), (18-21), and (31-34) represent the axial or star points for different tool diameter levels. The central points for different tool diameter levels in the design are reflected by experiment numbers (9-13), (22-26), and (35-39). The selected output responses for the straight groove tests were the theoretical depth of the groove (TD), spring back (SB), and forming time (FT), as defined by Equations (1a–1c).

$$TD\ (\text{mm}) = N\Delta Z \tag{1a}$$

$$FT(\text{s}) = \frac{80N}{V} \tag{1b}$$

$$SB(\%) = 100 \times \frac{TD - AD}{TD} \tag{1c}$$

Where, N is the no of passes to fracture, V is the peripheral speed of the tool ,TD is the theoretical depth and AD is the actual depth of the groove.

2.1. Results of Straight Grove Tests

39 Different experiments were carried out to find out the effect of different parameters on responses in the experiments to find out the optimal combination of tool speed, step size and tool diameter for further experimentation and analysis.Based on the design of experiments, a linear correlation was evaluated for the preliminary behaviour of output responses on the factors. The Pearson's correlation coefficient matrix is given in Table 5.

As can be seen from Table 5, the theoretical depth shows a weak negative correlation with tool speed (r = -0.375) and step size (r = -0.197), and a negligible correlation with tool diameter (r = -0.034). Forming time is moderately negatively correlated with tool speed (r = -0.409) and strongly negatively correlated with step size (r = -0.805), but shows no correlation with tool diameter (r = 0.006) which is very natural. Spring back exhibits a weak negative correlation with tool speed (r = -0.397) and negligible correlations with step size (r = -0.049) and tool diameter (r = -0.074). These results are limited by their reliance on Pearson linear correlations, as indicated by the confidence intervals. Hence, CCRSD was implemented using a higher-order model to capture nonlinear interactions. The process involved selecting parameters, defining experimental levels, and constructing a design matrix with factorial, axial, and center points. The collected data was then used to fit a second-order response surface model given by equation 2

$$Y = \beta_0 + \sum \beta_i X_i + \sum \beta_{ii} X_i^2 + \sum \beta_{ij} X_i X_j + \varepsilon \tag{2}$$

The model significance was assessed using ANOVA, and the accuracy was evaluated using the coefficient of determination (R^2) given by equation 3

$$R^2 = 1 - \frac{SSE}{SST} \tag{3}$$

where SSE is sum of square of errors and SST is tol sum of squares given by equations 4a and 4b respectively.

$$SSE = \sum (Y_i - \hat{Y}_i)^2 \tag{4a}$$

$$SST = \sum (Y_i - \bar{Y}_i)^2 \tag{4b}$$

To account for model complexity, the adjusted R^2 is computed as:

$$R^2_{\text{adj}} = 1 - \left(\frac{SSE/(n-p-1)}{SST/(n-1)} \right) \tag{5}$$

where n is the number of observations and p is the number of predictors. Additionally, the predicted R^2, which evaluates the model's predictive performance, is given by:

$$R^2_{\text{pred}} = 1 - \frac{\sum (Y_i - \hat{Y}_{\text{pred},i})^2}{SST} \tag{6}$$

Ex No	V (mm/s)	ΔZ (mm)	D (mm)	Theoretical Depth (mm)	Spring Back (%)	Forming time (s)
1	50.00	0.20	10.00	19.20	8.91	153.60
2	100.00	0.20	10.00	20.80	7.28	83.20
3	50.00	0.60	10.00	18.60	9.52	49.60
4	100.00	0.60	10.00	18.00	5.92	24.00
5	39.64	0.40	10.00	18.80	4.63	94.84
6	110.36	0.40	10.00	18.40	5.60	33.35
7	75.00	0.12	10.00	19.45	9.63	177.07
8	75.00	0.68	10.00	19.12	10.09	29.87
9	75.00	0.40	10.00	20.80	6.92	55.47
10	75.00	0.40	10.00	21.20	7.08	56.53
11	75.00	0.40	10.00	20.40	6.13	54.40
12	75.00	0.40	10.00	20.00	7.15	53.33
13	75.00	0.40	10.00	21.20	7.29	56.53
14	50.00	0.20	12.50	20.40	7.70	163.20
15	100.00	0.20	12.50	19.20	6.28	76.80
16	50.00	0.60	12.50	18.60	8.53	49.60
17	100.00	0.60	12.50	17.40	5.29	b23.20
18	39.64	0.40	12.50	19.20	5.94	96.86
19	110.36	0.40	12.50	17.60	4.66	31.90
20	75.00	0.12	12.50	21.32	5.52	194.13
21	75.00	0.68	12.50	19.80	9.05	30.93
22	75.00	0.40	12.50	20.00	5.45	53.33
23	75.00	0.40	12.50	21.60	6.23	57.60
24	75.00	0.40	12.50	22.00	8.14	58.67
25	75.00	0.40	12.50	20.80	6.61	55.47
26	75.00	0.40	12.50	21.20	5.73	56.53
27	50.00	0.20	15.00	20.80	7.14	166.40
28	100.00	0.20	15.00	18.40	6.28	73.60
29	50.00	0.60	15.00	19.20	9.56	51.20
30	100.00	0.60	15.00	18.00	4.69	24.00
31	39.64	0.40	15.00	18.00	7.19	90.81
32	110.36	0.40	15.00	18.00	6.94	32.62
33	75.00	0.12	15.00	20.03	8.16	182.40
34	75.00	0.68	15.00	17.75	5.96	27.73
35	75.00	0.40	15.00	20.80	8.05	55.47
36	75.00	0.40	15.00	21.20	9.08	56.53
37	75.00	0.40	15.00	20.40	7.99	54.40
38	75.00	0.40	15.00	21.60	6.18	57.60
39	75.00	0.40	15.00	20.40	7.25	54.40

Table 4: Details of experiments for CCRSD

By implementing this algorithm, the best process conditions were determined, ensuring maximum formability while minimizing defects. A detailed description of the same is given in forthcoming section.

2.1.1. Effect on theoretical depth

The theoretical depth (TD) of the groove can be calculated by equation 1a which is a direct representation of formability obtained in the experiment [18, 26]. The results of CCRSD for theoretical depth are presented

Interaction	r- value (r)	Confidence Interval (CI)
Theoretical depth – Tool Speed	-0.375	(-0.617, -0.067)
Theoretical depth – Step Size	-0.197	(-0.483, 0.126)
Theoretical depth – Tool Diameter	-0.034	(-0.346, 0.285)
Forming Time – Tool Speed	-0.409	(-0.641, -0.107)
Forming Time – Step Size	-0.805	(-0.894, - 0.657)
Forming Time – Tool Diameter	0.006	(-0.310, 0.321)
Spring Back – Tool Speed	-0.397	(-0.634, -0.094)
Spring Back – Step Size	-0.049	(-0.359, 0.271)
Spring Back – Tool Diameter	-0.074	(-0.248, 0.380)

Table 5: Details of various interactions between factors-responses in CCRSD

in Figure 2. The coefficient of determination, R^2, was found to be 84.87% whereas the adjusted and predicted R^2 value were found to be 78.71% and 64.41% respectively which exhibit the effectiveness of the model in predicting the behaviour of responses. Main Effects Plot for Theoretical Depth shows that tool speed and step size have a non-linear relationship with theoretical depth, with both exhibiting a peak at intermediate levels as depicted in Figure 2a. The interaction plot indicates significant interactions between tool speed and step size, as well as between tool speed and tool diameter . Similar findings have been reported by Kim and Park [18], Shim and Park [16]. The surface plot shown in figure 2c, further confirms the non-linearity, especially in the combined influence of tool speed and step size on theoretical depth. It can be concluded that in the small speed (38–55 mm/s) region with small step sizes (0.12–0.3 mm), the theoretical depth is on the lower side, due to limited local heating of the sheet. As the speed increases coupled with intermediate step size, formability becomes better and shows a peak somewhere in the central region (65–85 mm/s). In this speed range, the sheet softening due to local friction heating is predicted to be maximum. Post this speed and step size, the theoretical depth of the groove and thus the formability obtained decreases. Larger step sizes (> 0.5 mm) can lead to dynamic impact loading of the sheet at the corner leading to premature failure of the sheet [20, 22].The contour plot shown in figure 2d exhibits that intermediate tool speeds (approximately 65–85 mm/s) combined with step sizes around 0.3 to 0.4 units result in the greatest theoretical depth. The tool diameter of 12.5 mm resulted the best results of theoretical depth out of the three tools available.

2.1.2. Effect on forming time

The forming time of a given experiment has been calculated by equation 1b which is an essential parameter affecting the process capability. One of the limitations of ISF is its speed of fabrication, and hence, forming time was included as a parameter for optimization of the output responses. The response of forming time is straight forward. Forming time has a strong negative correlation with forming speed and step size as reported in Table 5. The main effect, interaction and surface plots of forming time are shown in Figure 3. As can be seen from Figure 3, the relation of forming time with tool speed and step size follows a negative trend (monotonically decreasing for tool speed). This decrease in trend is also reflected in the surface plot of forming time with tool speed and step size by the absence of curvature. The R^2, adjusted and predicted R^2 values were found to be 97.79%, 96.89% and 93.36% respectively which shows the effectiveness of the model in predicting the effect of forming time on the behaviour of responses.

2.1.3. Effect on spring back

As the metal is deformed plastically, the total strain has always some elastic component present in it, a part of which is recovered as the material is unloaded. This leads to spring back, which is a characteristic feature of almost all metal forming processes [38, 39]. The spring back occurring in the straight groove test has been evaluated by equation 1c.The results of CCRSD used for the spring back are shown in Figure 4. The R^2 and adjusted R^2 values were found to be 51.30% and 31.46% respectively which show that the model does not have a strong capability to predict the outcome of the experiments. However, it can be loosely said that the spring back decreases with increasing speed in a higher speed range (> 60 mm/s). The variation of spring back with step size follows a near well curve pattern whose minimum is observed in the region of central points in CCRSD. It can be concluded that, further study is needed to predict the spring back behaviour in ISF, and intelligent predictive [40]and compensation models [41, 42] using neural networks and machine learning [37] should be incorporated for im-

effects plot for theoretical depth.png

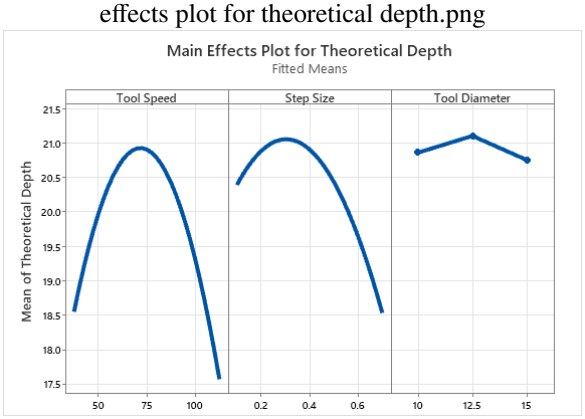

effects plot for theoretical depth.png

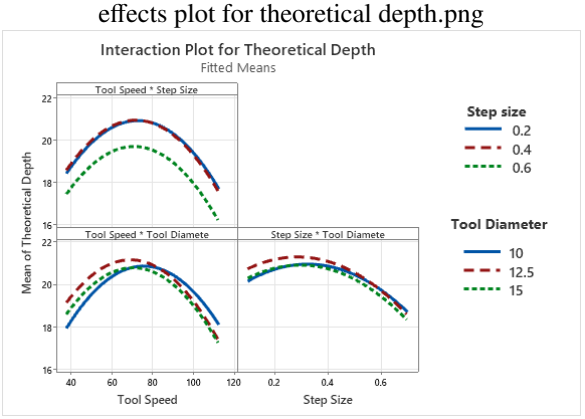

Plot of Theoretical Depth vs Step Size, Tool Speed.png

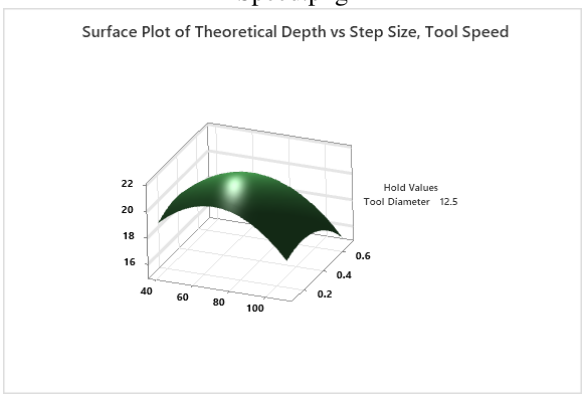

Plot of Theoretical Depth vs Step Size, Tool Speed.png

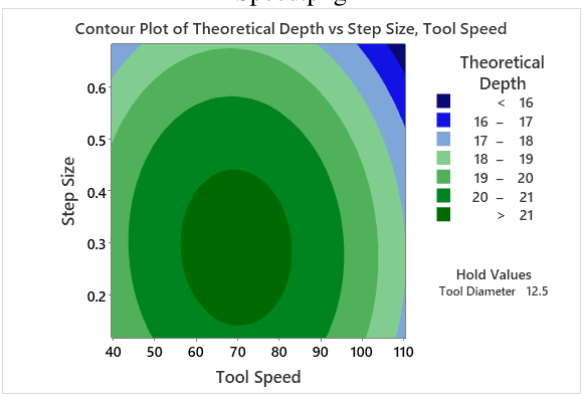

(a)

Figure 2: Analysis of theoretical depth: (a) main effect plot using, (b) interaction effect plot using non linear interpolation,(c) surface plot at hold tool diameter 12.5mm and (d) contour plot with step size and tool speed at hold tool diameter 12.5mm.

proving accuracy of prediction of the spring back behaviour.

2.2. *Optimization of Parameters*

Once the responses of different parameters were evaluated for different factors, the parameters were optimized constraining theoretical depth to maximum, and forming time and spring back to minimum. The details of optimized parameters along with the plot are presented in Table 6. As indicated in Table 6, the optimal combination of theoretical forming depth, forming time, and spring back can be achieved with a tool speed of 84.65 mm/s, a step size of 0.40 mm, and a tool diameter of 12.5 mm. The optimization of the parameters using regression method is depicted in figure 5. The composite desirability of fit for this combination is 0.765162, which is considered acceptable. These parameters were selected for further experiments.The regression equations for output responses are presented in equations (7–9),

$$\text{Depth } (D) = 9.86 + 0.2865V + 10.47\Delta Z - 0.002021V^2 - 16.02(\Delta Z)^2 - 0.0167V\Delta Z \quad (7)$$

$$\text{Time } (t) = 432.6 - 2.656V - 939.4\Delta Z + 0.00331V^2 + 597.1(\Delta Z)^2 + 2.840V\Delta Z \quad (8)$$

$$\text{Spring Back } (\%) = 1.56 + 0.1440V + 0.72\Delta Z - 0.000829V^2 + 15.06(\Delta Z)^2 - 0.1300V\Delta Z \quad (9)$$

It is important to emphasize that these specific values should not be applied indiscriminately in all experiments, as they are contingent on the type of ISF used, the materials being formed, and the parameters optimized. Nevertheless, the approach detailed in this work can be used as a template methodology for optimizing forming parameters.

effects plot for forming time.png

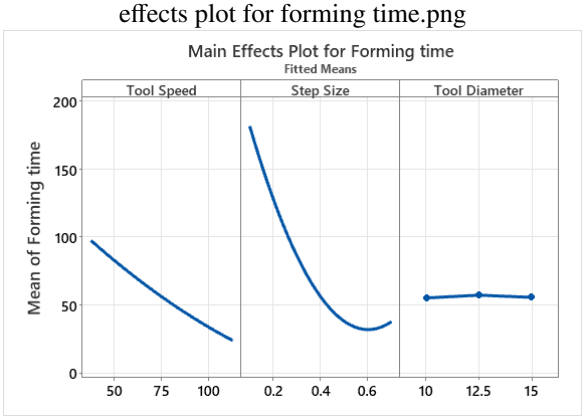

(a)

effects plot for forming time.png

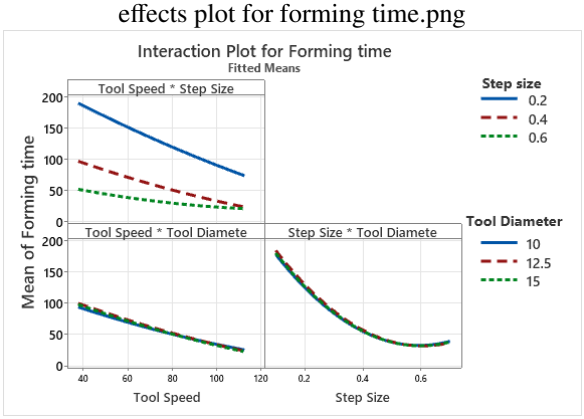

(b)

Plot of Forming time vs Step Size, Tool Speed.png

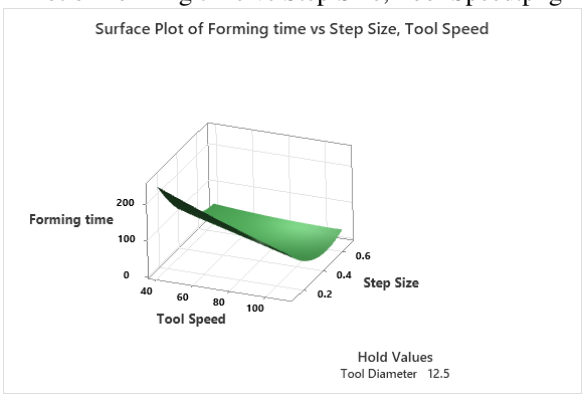

(c)

Plot of Forming time vs Step Size, Tool Speed.png

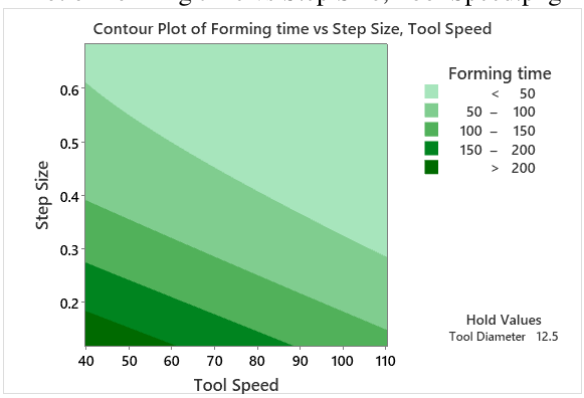

(d)

Figure 3: Analysis of forming time: (a) main effect plot using, (b) interaction effect plot using non linear interpolation,(c) surface plot at hold tool diameter 12.5mm and (d) contour plot with step size and tool speed at hold tool diameter 12.5mm.

Response	Goal	Lower	Target	Upper	Weight	
Forming time	Minimum		23.20	194.13	1	
Spring Back	Minimum		4.63	10.09	1	
Theoretical Depth	Maximum	17.4	22.00		1	
Solutions						
			Forming time	Spring back	Theoretical Depth	
Tool Speed	Step size	Tool Diameter	Fit	Fit	Fit	CD
84.65	0.39	12.50	48.04	6.10	20.70	0.76

Table 6: Details of optimized parameters

3. Forming Limits

3.1. Conical Frustrams

Once the optimal parameters were chosen using CCRSD, they were selected to make various shapes using RAISF [31]. A fixed angle conical frustum has been widely used by researchers to examine the formability of the process. To find out the maximum limit of the wall angle of conical frustum, a variable wall angle conical frustum (VWACF) was used, as recommended by Hussain et al. [26] and shown in Figure 6. The limiting wall angle was found to be 60°, and finally a conical frustum of wall angle 60^0 was fabricated using the optimized parameters. To accurately quantify strain in the plane of the sheet during the formation of the cone, a circular grid pattern with 10 mm diameter (D_0) circles was imprinted onto the sheet metal using a 50 W fibre laser [36, 43], as shown in Figure 6(d), and was divided into seven regions. Region zero was the un-

Effects Plot for Spring Back.png

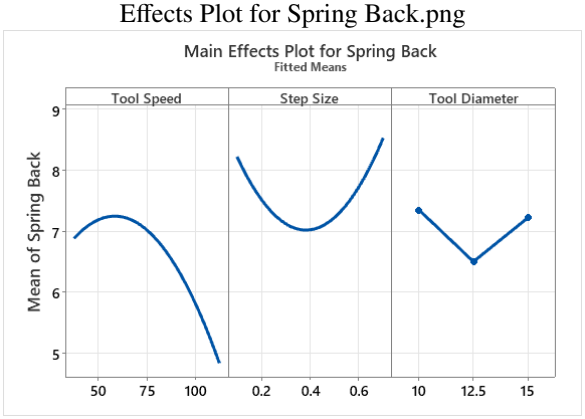

(a)

Plot for Spring Back.png

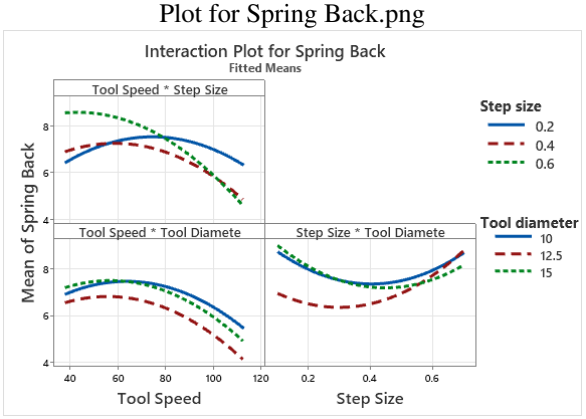

(b)

Plot of Spring Back vs Step Size, Tool Speed.png

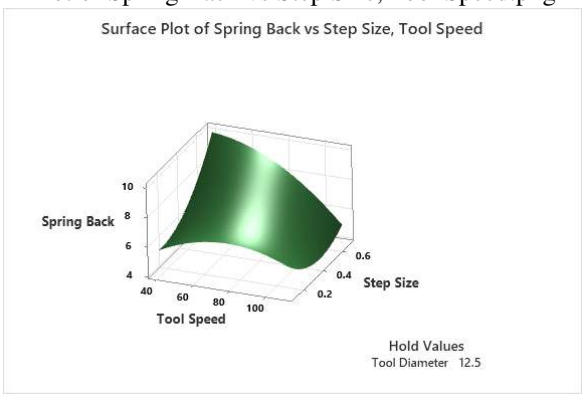

(c)

Plot of Spring Back vs Step Size, Tool Speed.png

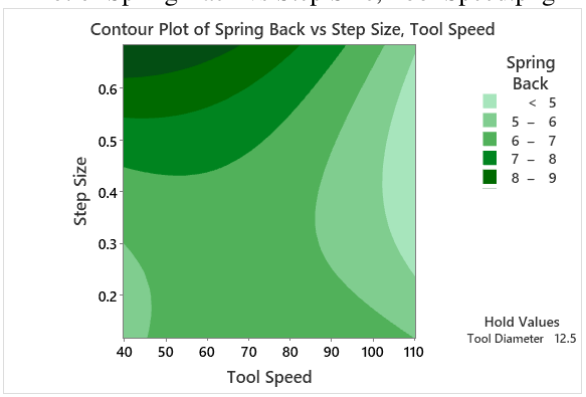

(d)

Figure 4: Analysis of spring back: (a) main effect plot using, (b) interaction effect plot using non linear interpolation,(c) surface plot at hold tool diameter 12.5mm and (d) contour plot with step size and tool speed at hold tool diameter 12.5mm.

Plot.png

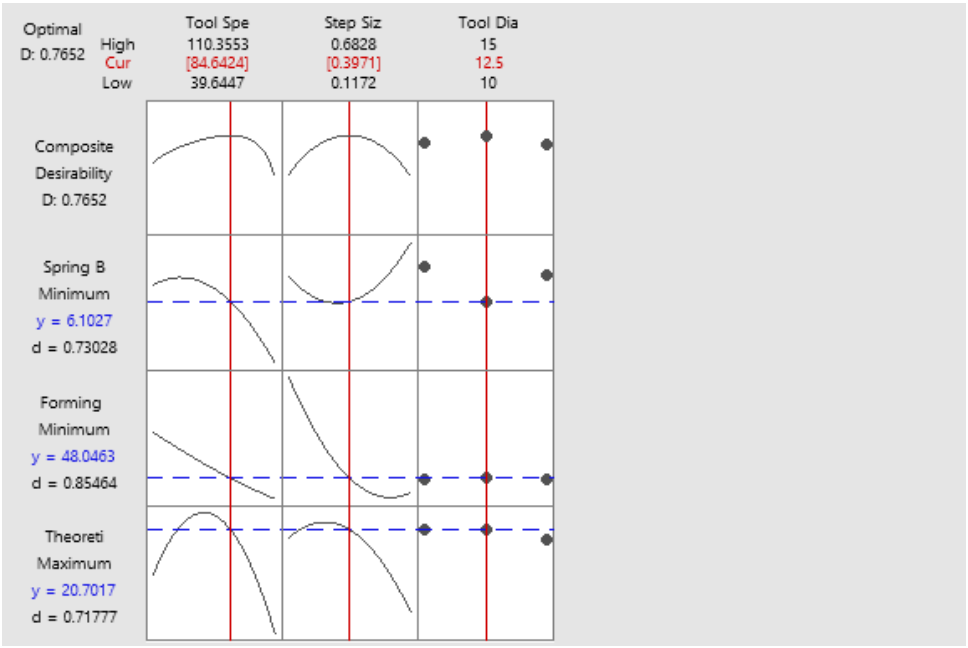

Figure 5: Optimization plot for Tool diameter, Tool speed and step size

deformed region at the base of the cone and region 6 was the region of largest material accumulation at the vertex of the cone. After deformation the circular pattern became elliptical, and the major and the minor

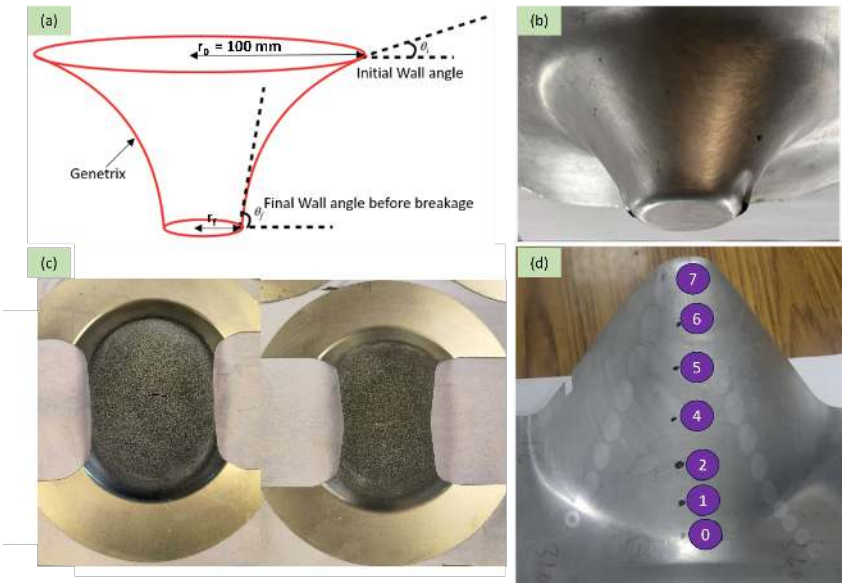

for ISF.png

Figure 6: (a) Genetrix of VWACF, (b) fabricated VWACF, (c) fractured samples during Nakazima test and (d) cone with circles distorted into ellipses.

axes of which were measured using optical microscope by taking a slice along the lenth of cone containing distorted patterns, for strain analysis on major strain-minor strain space. True major and minor strains were calculated by equations 10a and 10b respectively.

3.2. Nakajima Tests

The major strains and minor strains obtained in the ISF were compared with the formability of the material evaluated in terms of the forming limit curve (FLC). The standard FLC was measured according to the ISO 12004-2: 2008 standard [44] using the Nakajima test. During the test, a hemispherical punch with a diameter of 100 mm was used to perform out-of-plane stretching on a series of sample geometries to generate different strain paths, as shown in Figure 7, in an ITC Interlaken 1000 kN hydraulic press, equipped with a Nakajima punch and smooth clamp ring set [45].

The sample in Figure 7(a) generates an equi-biaxial strain path, while the sample in Figure 7(g) generates a uniaxial strain path. The samples in between produce other strain paths, ranging between these two extremes, including biaxial and plane strain paths. Figure 7(h) shows the orientation of the specimen geometries during the tests.A minimum of three repeats were carried out for each sample geometry. Friction was minimized on the punch by applying a lubrication stack (tallow/Teflon/tallow/PVC/tallow/Teflon/tallow layers) between the specimen and the punch. The failure strain was measured with a GOM 5M digital image correlation (DIC) system using a position-dependent method. The DIC system consisted of two 5MP cameras fitted with 50 mm lenses to capture images of the sample surface at a frame rate of 20 frames per second. A speckled paint pattern was applied to the sample surface before the test, and GOM ARAMIS version 6.1 software was used to acquire and process the captured images to calculate strain [46].The broken samples with speckled paint pattern is shown in 6c. The calculated failure strain values were plotted on the Major-strain-minor strain space to represent the forming limit curve (FLC) of the material, as shown in Figure 8.

3.3. Forming Limit Comparisons

Figure 8 also plots, in the same strain–strain space, the scatter plot of major strain and minor strain from the forming limit obtained from RAISF for the 60° fixed angle conical frustum, calculated by

$$Major\ strain = log\left(\frac{D_1}{D_0}\right) \tag{10a}$$

$$Minor\ strain = \left(\frac{D_2}{D_0}\right) \tag{10b}$$

It can be seen from Figure 8 that in-plane strains obtained in RAISF are well above the strains obtained in various loading paths during the Nakajima test. The attainment of higher strain is one of the key benefits of ISF over traditional forming operations which is attributed to localized nature of deformation and, thereby, suppression/ delay of necking. Factors such as the nature of stress triaxiality at contact, bending under tension, shear, cyclic straining, and the geometrical inability of the neck to grow result in the delay in the necking [47, 48].

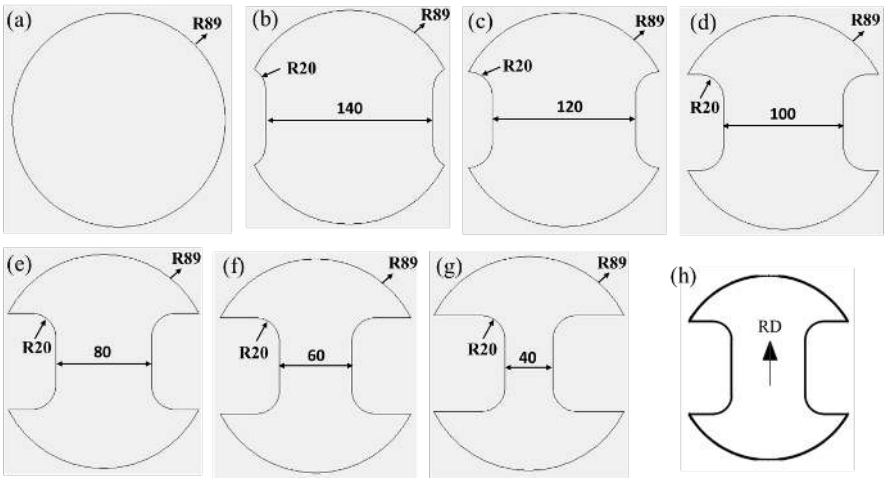

samples.png

Figure 7: (a-g) Specimen geometries for the generation of FLC and (h) preferred orientation of the specimens used in FLC testing.

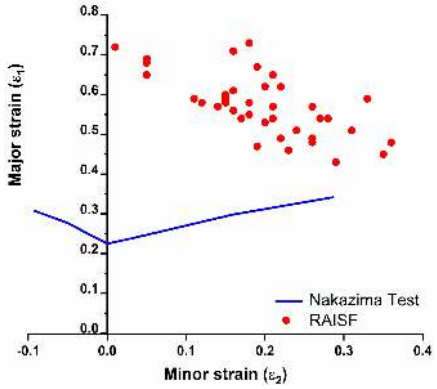

Figure 8: Strains obtained from the RAISF and forming limit curve (FLC) of the material obtained from the Nakajima test.

4. Conclusions

In the current work, a simplified but innovative approach has been presented for process optimization for formability evaluation in RAISF. Based on the studies undertaken in the current article, a simplified approach for formability optimization and evaluation in RAISF is summarized in figure 9.

The methodology utilizes a simple straight groove test and CCRSD for optimization of parameters and VWACF test for finding out the limiting wall angle of the shapes to be formed. The approach can be pivotal in designing the process in terms of tool speed, step size amd tool diameter used for fabricating various shapes using RAISF. A straight groove test was conducted on 39 samples for different combinations of tool speed, tool diameter and step depth. it was revealed from regression model using CCRSD, that these parameters have am impact on various output parameters such as forming depth of groove, spring back and forming time. A combination of input variables for maximum forming depth, minimal spring depth and forming time was evaluated using CCRSD and the optimal combination of tool speed (84.65 mm/s), tool diameter (12.5 mm) and step depth (0.4 mm) were obtained which was used for further experimentations. Further, VWACF was used to find out the limiting wall angle of the conical frustum. A fixed angle conical frustum of the limiting wall angle as obtained from VWACF was fabricated. The forming limit obtained in RAISF was obtained using the gridding methodology and was compared with the conventional forming limit of AA6061 using the Nakajima test on major strain-minor strain space. It was revealed that, significantly high level of in plane plain strain was obtained in case of RAISF than conventional sheet metal forming operations.

Acknowledgement

The authors are grateful to DST-SERB for sponsoring the work through project MMER/2014/0068 titled ‘Design, Development and Fabrication of an Incremental sheet hydroforming machine setup’.

Data Availability statement

The raw/processed data required to reproduce these findings cannot be shared at this time as the data also forms part of an ongoing study.

Consent for publication

Consent for publication was obtained from all participants.

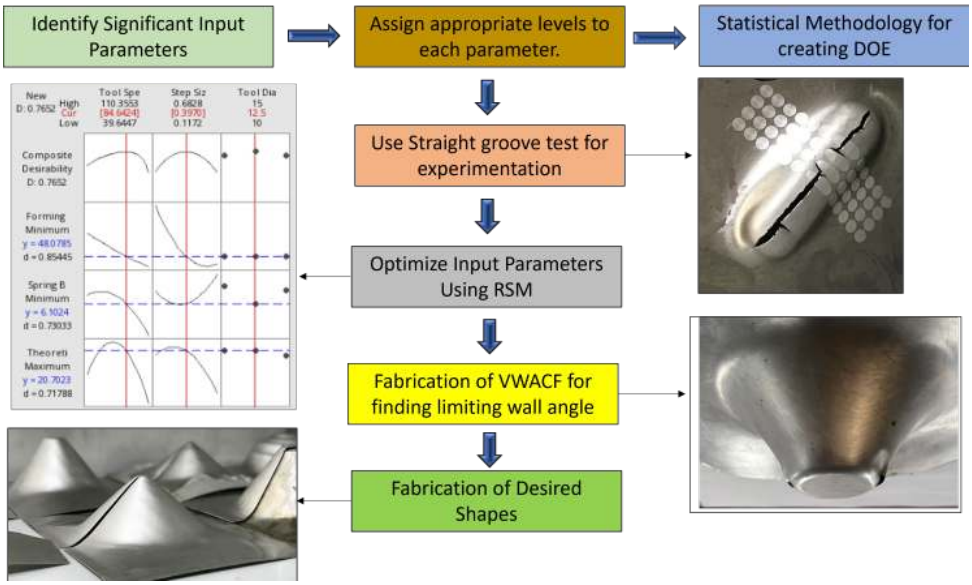

Figure 9: Proposed methodology for formability evaluation in RAISF.

Conflict of interest

The authors declare that they have no conflict of interest

References

[1] Jeswiet, Micari, Hirt, Bramley, Duflou, and Allwood, (2005). "Asymmetric single point incremental forming of sheet metal". *CIRP annals*, **54**(2) 88–114.

[2] Ziran, Gao, Hussain, and Cui, (2010). "The performance of flat end and hemispherical end tools in single-point incremental forming". *The International Journal of Advanced Manufacturing Technology*, **46** 1113–1118.

[3] Leszak, (1967). "Apparatus and process for incremental dieless forming". US Patent 3342051 A. `https://lens.org/177-750-492-332-96X`.

[4] Chang, Huang, and Chen, (2020). "A new tool path with point contact and its effect on incremental sheet forming process". *The International Journal of Advanced Manufacturing Technology*, **110** 1515–1525.

[5] Kumar, Mehtani, Shrivastava, Mishra, Narasimhan, and Samajdar, (2023). "Failure mechanism during incremental sheet forming of a commercial purity aluminum alloy". *Engineering Failure Analysis*, **146** 107090.

[6] Singh, Gupta, Singh, and Kumar, (2021). "Robot assisted incremental sheet forming of al6061 under static pressure: Preliminary study of thickness distribution within the deformation region". *Materials Today: Proceedings*, **47** 2737–2741.

[7] Jackson and Allwood, (2009). "The mechanics of incremental sheet forming". *Journal of materials processing technology*, **209**(3) 1158–1174.

[8] Ismail, Ismail, Radzman, Ariffin, and Asárry, (2019). "Parametric optimization of robot-based single point incremental forming using taguchi method". *International Journal of Integrated Engineering*, **11**(1).

[9] Ismail, Ismail, Ariffin, and As'arry, (2020). "Surface characterization of heat-affected zone in robot-based increment sheet forming". *Journal Tribology*, **24** 126–134.

[10] Mohanty, Regalla, and Daseswara Rao, (2019). "Robot-assisted incremental sheet metal forming under the different forming condition". *Journal of the Brazilian Society of Mechanical Sciences and Engineering*, **41** 1–12.

[11] Mohanty, Regalla, and YV, (2018). "Investigation of influence of part inclination and rotation on surface quality in robot assisted incremental sheet metal forming (raisf)". *CIRP Journal of Manufacturing Science and Technology*, **22** 37–48.

[12] Kim and Yang, (2000). "Improvement of formability for the incremental sheet metal forming process". *International Journal of Mechanical Sciences*, **42**(7) 1271–1286.

[13] Park and Kim, (2003). "Fundamental studies on the incremental sheet metal forming technique". *Journal of Materials Processing Technology*, **140**(1-3) 447–453.

[14] McAnulty, Jeswiet, and Doolan, (2017). "Formability in single point incremental forming: A comparative analysis of the state of the art". *CIRP Journal of Manufacturing Science and Technology*, **16** 43–54.

[15] Huang, Wang, Cao, and Li, (2007). "Prediction of forming limit in single point incremental forming with the ductile fracture criterion". In *International Manufacturing Science and Engineering Conference*, volume 42908, pages 929–934.

[16] Shim and Park, (2001). "The formability of aluminum sheet in incremental forming". *Journal of Materials Processing Technology*, **113**(1-3) 654–658.

[17] Ham and Jeswiet, (2006). "Single point incremental forming and the forming criteria for aa3003". *CIRP annals*, **55**(1) 241–244.

[18] Kim and Park, (2002). "Effect of process parameters on formability in incremental forming of sheet metal". *Journal of materials processing technology*, **130** 42–46.

[19] Kumar, Gulati, Kumar, Singh, Kumar, and Singh, (2019). "Parametric effects on formability of aa2024-o aluminum alloy sheets in single point incremental forming". *Journal of Materials Research and Technology*, **8**(1) 1461–1469.

[20] Shanmuganatan and Kumar, (2013). "Metallurgical analysis and finite element modelling for thinning characteristics of profile forming on circular cup". *Materials & Design*, **44** 208–215.

[21] Centeno, Bagudanch, Martínez-Donaire, Garcia-Romeu, and Vallellano, (2014). "Critical analysis of necking and fracture limit strains and forming forces in single-point incremental forming". *Materials & Design*, **63** 20–29.

[22] Golabi and Khazaali, (2014). "Determining frustum depth of 304 stainless steel plates with various diameters and thicknesses by incremental forming". *Journal of Mechanical Science and Technology*, **28** 3273–3278.

[23] Ullah, Li, Li, Xu, and Li, (2022). "A review on the deformation

mechanism and formability enhancement strategies in incremental sheet forming". *Archives of Civil and Mechanical Engineering*, **23**(1) 55.

[24] Trzepieciński, Szpunar, Dzierwa, and Żaba, (2022). "Investigation of surface roughness in incremental sheet forming of conical drawpieces from pure titanium sheets". *Materials*, **15**(12) 4278.

[25] Mulay, Ben, Ismail, Kocanda, and Jasiński, (2018). "Performance evaluation of high-speed incremental sheet forming technology for aa5754 h22 aluminum and dc04 steel sheets". *Archives of Civil and Mechanical Engineering*, **18** 1275–1287.

[26] Hussain, Gao, Hayat, and Dar, (2010). "The formability of annealed and pre-aged aa-2024 sheets in single-point incremental forming". *The International Journal of Advanced Manufacturing Technology*, **46** 543–549.

[27] Buffa, Campanella, and Fratini, (2013). "On the improvement of material formability in spif operation through tool stirring action". *The International Journal of Advanced Manufacturing Technology*, **66** 1343–1351.

[28] Xu, Wu, Malhotra, Chen, Lu, and Cao, (2013). "Mechanism investigation for the influence of tool rotation and laser surface texturing (lst) on formability in single point incremental forming". *International Journal of Machine Tools and Manufacture*, **73** 37–46.

[29] Jain, Kagzi, Patel, and Vasava, (2021). "An analysis of the effect of various parameters on surface roughness, springback and thinning while performing single point incremental forming on polypropylene sheet". *Proceedings of the Institution of Mechanical Engineers, Part E: Journal of Process Mechanical Engineering*, page 09544089211047203.

[30] Kumar and Kumar, (2017). "Robot assisted high speed incremental sheet hydroforming machine". Patent application no. 201711011951.

[31] Singh, Kumar, Singh, Meraz, and Salunkhe, (2024). "Advancements in robot-assisted incremental sheet hydroforming: a comparative analysis of formability, mechanical properties, and surface finish for rhomboidal and conical frustums". *International Journal of Intelligent Robotics and Applications*, pages 1–13.

[32] Singh, Kumar, Pande, Salunkhe, Ragab, Singh, Meraz, and Davim, (2023). "Robot-assisted cold and warm incremental sheet forming of aluminum alloy 6061: a comparative study". *Metals*, **13**(3) 568.

[33] ASTM E8/E8M-15a. *Standard Test Methods for Tension Testing of Metallic Materials*. ASTM International, West Conshohocken, PA, (2015). `https://www.astm.org`.

[34] ASTM E643-15. *Standard Test Method for Ball Punch Deformation of Metallic Sheet Material*. ASTM International, West Conshohocken, PA, (2015).

[35] Hussain, Hayat, and Lin, (2012). "Pyramid as test geometry to evaluate formability in incremental forming: Recent results". *Journal of mechanical science and technology*, **26** 2337–2345.

[36] Keeler, (1978). "Forming limit criteria—sheets". In *Advances in deformation processing*, pages 127–157. Springer.

[37] Choudhary, Choudhary, Kumari, Kumari, and Mulay, (2025). "Application of artificial neural network in predicting the performance of spif for aerospace grade aa7075-t6". *Journal of Alloys and Compounds*, **1010** 177146.

[38] Bosetti and Bruschi, (2011). "Springback evaluation of parts made by single-point incremental sheet forming". In *ASME International Mechanical Engineering Congress and Exposition*, volume 54891, pages 925–932.

[39] Vahdati and Vahdati, (2011). "Experimental, statistical and simulation study on spring-back behavior in incremental sheet metal forming (ismf) process". In *AIP Conference Proceedings*, volume 1315, pages 607–612. American Institute of Physics.

[40] Khan, Coenen, Dixon, El-Salhi, Penalva, and Rivero, (2015). "An intelligent process model: predicting springback in single point incremental forming". *The International Journal of Advanced Manufacturing Technology*, **76** 2071–2082.

[41] Yan, Meng, Zhu, Wang, and Wan, (2024). "A global springback compensation method for manufacturing metallic seal ring with complex cross-section and submillimeter precision". *Journal of Materials Processing Technology*, **331** 118498.

[42] Su, Jiang, and Xiong, (2020). "Multi-point forming springback compensation control oftwo-dimensional hull plate". *Advances in Mechanical Engineering*, **12**(4) 1687814020916094.

[43] Ham and Jeswiet, (2007). "Forming limit curves in single point incremental forming". *CIRP annals*, **56**(1) 277–280.

[44] Banabic, Lazarescu, Paraianu, Ciobanu, Nicodim, and Comsa, (2013). "Development of a new procedure for the experimental determination of the forming limit curves". *CIRP Annals*, **62** (1) 255–258.

[45] Taylor, Masters, Li, and Kotadia, (2019). "Comparison of formability and microstructural evolution of c106 copper and 316l stainless steel". *JOM*, **71** 2721–2727.

[46] Sutton, Orteu, and Schreier, (2009). *Image correlation for shape, motion and deformation measurements: basic concepts, theory and applications*. Springer Science & Business Media.

[47] Gatea, Ou, and McCartney, (2016). "Review on the influence of process parameters in incremental sheet forming". *The International Journal of Advanced Manufacturing Technology*, **87** 479–499.

[48] Emmens and van den Boogaard, (2009). "An overview of stabilizing deformation mechanisms in incremental sheet forming". *Journal of Materials Processing Technology*, **209**(8) 3688–3695.